Analysis of Current Density Distributions over the Cross-Section of OPGW Cables Using an Analytical Model and the FEM Numerical Method

João T. Pinho[1], Victor Dmitriev[1], Karlo Q. da Costa[1], Luciana Gonzalez[1], Sérgio Colle[2], Marcelo A. Andrade[3], João C. V. da Silva[3], Mauro Bedia[3]

[1]Department of Eletrical Engineering/ Federal University of Pará, Belém, Pará/Brasil, jtpinho@ufpa.br/+55-91-32017299, [1]Department of Mechanical Engineering/ Federal University of Santa Catarina, Florianópolis, Santa Catarina/ Brasil, colle@emc.ufsc.br/ + 55-48-32342161, [3]Prysmian Telecomunicações, Cabos e Sistemas do Brasil S.A, Sorocaba, São Paulo/Brazil, marcelo.andrade@prysmian.com/ +55-15-32359209

Abstract — **Multiconductor OPGW cables have a double function: they serve for lightning protection and as a communications channel. In this work, we present some results of the analysis of current density distributions in these cables obtained by an analytical method and using the FEMLAB software.**

Index Terms — **Cables, waveguide theory, current density.**

I. Introduction

OPGW (optical ground wire) cables provide lightning protection for overhead power lines and also serve as a fiber optic cable for high performance telecommunication network. These cables are composed of an envelope of one or two layers of metallic helical wires wound around a core containing optical fibers. The metallic helical wires can be of the type aluminized steel, aluminum welds or galvanized steel.

We consider a variant of such cables consisting of three layers: dielectric in the core, aluminum in the intermediate layer and steel in the last layer. This structure is shown in Fig. 1.

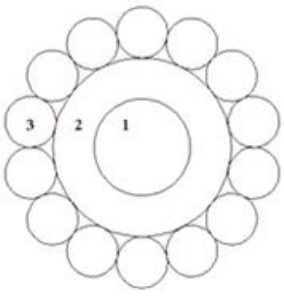

Fig. 1. The real geometry of the cable's cross-section.

During the occurrence of short circuits or lightning, the thermal gradient that occurs in the cable can produce plastic deformations, rupture, and the phenomenon of caging.

The thermal gradient depends on the current distribution in the cable. In this paper, the goal is to calculate the current density distribution in the OPGW cable using an analytical model based on Maxwell's equations, and using the software FEMLAB [1]. The following analysis of the current density distribution is performed in the frequency domain. Analytical calculations of current distributions of OPGW cables can be found in [2-3].

II. Analytical Model

Our analytical model of OPGW cable consists of four homogeneous layers: 1-dielectric, 2-aluminium, 3-steel and 4-air. This configuration is shown in Fig.2. The conductivities of the dielectric and metal layers are finite. The waveguide is analyzed by Maxwell´s equations in the frequency domain.

The eigenvalue problem is considered. Due to the cylindrical symmetry of the problem, we consider the electromagnetic modes TM^{z}_{0n} that are not changed with respect to the azimuthal coordinate ϕ , i.e. $\frac{\partial}{\partial \phi} = 0$ and n is a nonnegative integer [2].

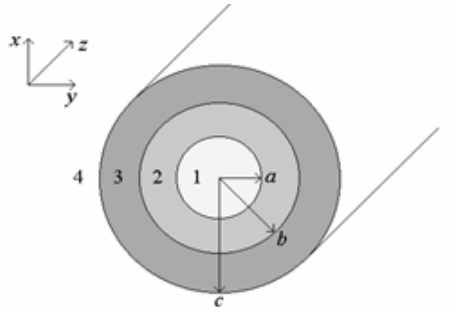

Fig. 2. Cross section geometry of the analytical model.

The parameters used for calculations of this structure are given in Table 1.

TABLE 1
PARAMETERS USED FOR ANALYTICAL MODEL

Layer	Material	Conductivity (S/m) (σ)	Relative permittivity	Radius (mm)
1	Silica	0	3.8	2.8
2	Aluminum	3.96×10^{7}	1	4.1
3	Steel	0.2×10^{7}	1	7.2
4	Air	0	1	-

To find the solutions for the electromagnetic fields, Maxwell´s equations in cylindrical coordinate system in the frequency domain are used. Considering the TM^z modes, one obtains:

$$\frac{\partial E_\rho}{\partial z}-\frac{\partial E_z}{\partial \rho}=-j\omega\mu H_\phi\,, \tag{1}$$

$$\frac{\partial H_\phi}{\partial z}=-j\omega\varepsilon E_\rho\,, \tag{2}$$

$$\frac{1}{\rho}\frac{\partial(\rho H_\phi)}{\partial \rho}=j\omega\varepsilon E_z\,, \tag{3}$$

where $\varpi=2\pi f$ is the angular frequency, f is the frequency in Hz, μ and ε are, respectively, the magnetic permeability and the electric permittivity of the layers (Fig.1).

Assuming the variation in z given by $e^{-jk_z z}$, the components of the fields can be written as follows

$$E_\rho(\rho,z)=E_\rho(\rho)e^{-jk_z z}\,, \tag{4}$$

$$E_z(\rho,z)=E_z(\rho)e^{-jk_z z}\,, \tag{5}$$

$$H_\phi(\rho,z)=H_\phi(\rho)e^{-jk_z z}\,. \tag{6}$$

Using the expressions (1)-(3), the following equations are obtained:

$$-jk_z E_\rho-\frac{\partial E_z}{\partial \rho}=-j\omega\mu H_\phi\,, \tag{7}$$

$$E_\rho=\frac{k_z}{\omega\varepsilon}H_\phi\,, \tag{8}$$

$$E_z=\frac{1}{j\omega\varepsilon}\frac{1}{\rho}\frac{\partial(\rho H_\phi)}{\partial \rho}\,. \tag{9}$$

Substituting (8) and (9) in (7), the differential equation for the H_ϕ component is obtained:

$$\frac{d}{d\rho}\left[\frac{1}{\rho}\frac{d(\rho H_\phi)}{d\rho}\right]+\lambda^2 H_\phi=0\,, \tag{10}$$

where $\lambda^2=k^2-k_z^2=\omega^2\mu\varepsilon-k_z^2$. Substituting $x=\lambda\rho$ in this equation results the Bessel equation

$$\frac{d^2H_\phi}{dx^2}+\frac{1}{x}\frac{dH_\phi}{dx}+\left(1-\frac{1}{x^2}\right)H_\phi=0\,, \tag{11}$$

with the possible solutions in the form of Bessel, Hankel and modified Bessel functions. The general solutions for the fields H_φ and E_z in layers 1-4 are written in Table 2.

TABLE 2
GENERAL FIELD SOLUTIONS E_Z AND H_ϕ OF THE WAVEGUIDE

Fields (eigenfunctions)	Eigenvalue and constant of propagation
$\begin{cases}H_{\phi1}=C_1J_1(\gamma_1\rho)\\ E_{z1}=\dfrac{C_1\gamma_1}{j\omega\varepsilon_1}J_0(\gamma_1\rho)\end{cases}$	$\gamma_1^2=k_1^2-k_z^2$ $k_1=\omega\sqrt{\mu_0\varepsilon_1}$ $=\omega\sqrt{\mu_0\varepsilon_0\varepsilon_{r1}}$
$\begin{cases}H_{\phi2}=C_2J_1(\gamma_2\rho)+C_3Y_1(\gamma_2\rho)\\ E_{z2}=\dfrac{\gamma_2}{j\omega\varepsilon_2}[C_2J_0(\gamma_2\rho)+C_3Y_0(\gamma_2\rho)]\end{cases}$	$\gamma_2^2=k_2^2-k_z^2$ $k_2=\omega\sqrt{\mu_0\varepsilon_2}$ $=\omega\sqrt{\mu_0\left(\varepsilon_0\varepsilon_{r2}+\dfrac{\sigma_2}{j\omega}\right)}$
$\begin{cases}H_{\phi2}=C_2J_1(\gamma_2\rho)+C_3Y_1(\gamma_2\rho)\\ E_{z2}=\dfrac{\gamma_2}{j\omega\varepsilon_2}[C_2J_0(\gamma_2\rho)+C_3Y_0(\gamma_2\rho)]\end{cases}$	$\gamma_3^2=k_3^2-k_z^2$ $k_3=\omega\sqrt{\mu_0\varepsilon_3}$ $=\omega\sqrt{\mu_0\left(\varepsilon_0\varepsilon_{r3}+\dfrac{\sigma_3}{j\omega}\right)}$
$\begin{cases}H_{\phi2}=C_2J_1(\gamma_2\rho)+C_3Y_1(\gamma_2\rho)\\ E_{z2}=\dfrac{\gamma_2}{j\omega\varepsilon_2}[C_2J_0(\gamma_2\rho)+C_3Y_0(\gamma_2\rho)]\end{cases}$	$\gamma_4^2=k_4^2-k_z^2$ $k_4=\omega\sqrt{\mu_0\varepsilon_0}=\omega\sqrt{\mu_0\varepsilon_1}$

In this table, the indexes of each term refer to the corresponding layer.

The eigenvalue equation to determine the parameters γ_1- γ_4 presented in Table 2 is derived in this section. Using the general solutions presented in Table 2 and applying the boundary conditions of continuity of the fields E_z and H_ϕ at the surfaces $\rho=a$, b e c the following set of equations is obtained:

$$C_1J_1(\lambda_1 a)=C_2J_1(\lambda_2 a)+C_3Y_1(\lambda_2 a)\,, \tag{12}$$

$$C_2J_1(\lambda_2 b)+C_3Y_1(\lambda_2 b)=C_4J_1(\lambda_3 b)+C_5Y_1(\lambda_3 b)\,, \tag{13}$$

$$C_4J_1(\lambda_3 c)+C_5Y_1(\lambda_3 c)=C_6H_1^{(2)}(\lambda_4 c)\,, \tag{14}$$

$$\frac{C_1\lambda_1}{j\omega\varepsilon_1}J_0(\lambda_1 a)=\frac{\lambda_2}{j\omega\varepsilon_2}[C_2J_0(\lambda_2 a)+C_3Y_0(\lambda_2 a)]\,, \tag{15}$$

$$\frac{\lambda_2}{j\omega\varepsilon_2}[C_2J_0(\lambda_2 b)+C_3Y_0(\lambda_2 b)]=\frac{\lambda_3}{j\omega\varepsilon_3}[C_4J_0(\lambda_3 b)+C_5Y_0(\lambda_3 b)]\,, \tag{16}$$

$$\frac{\lambda_3}{j\omega\varepsilon_3}[C_4 J_0(\lambda_3 c) + C_5 Y_0(\lambda_3 c)] = \frac{C_6\lambda_4}{j\omega\varepsilon_4} H_0^{(2)}(\lambda_4 c) \tag{17}$$

To simplify the equations, the following notations are introduced:

$$\begin{aligned}
&x_1 = J_1(\lambda_1 a),\ x_2 = J_1(\lambda_2 a),\ x_3 = Y_1(\lambda_2 a),\\
&x_4 = J_1(\lambda_2 b),\ x_5 = Y_1(\lambda_2 b),\ x_6 = J_1(\lambda_3 b),\\
&x_7 = Y_1(\lambda_3 b),\ x_8 = J_1(\lambda_3 c),\ x_9 = Y_1(\lambda_3 c),\\
&x_{10} = H_1^{(2)}(\lambda_4 c),\ x_{11} = \frac{\lambda_1}{j\omega\varepsilon_1} J_0(\lambda_1 a),\\
&x_{12} = \frac{\lambda_2}{j\omega\varepsilon_2} J_0(\lambda_2 a),\ x_{13} = \frac{\lambda_2}{j\omega\varepsilon_2} Y_0(\lambda_2 a),\\
&x_{14} = \frac{\lambda_2}{j\omega\varepsilon_2} J_0(\lambda_2 b),\ x_{15} = \frac{\lambda_2}{j\omega\varepsilon_2} Y_0(\lambda_2 b),\\
&x_{16} = \frac{\lambda_3}{j\omega\varepsilon_3} J_0(\lambda_3 b),\ x_{17} = \frac{\lambda_3}{j\omega\varepsilon_3} Y_0(\lambda_3 b),\\
&x_{18} = \frac{\lambda_3}{j\omega\varepsilon_3} J_0(\lambda_3 c),\ x_{19} = \frac{\lambda_3}{j\omega\varepsilon_3} Y_0(\lambda_3 c),\\
&x_{20} = \frac{\lambda_4}{j\omega\varepsilon_4} H_0^{(2)}(\lambda_4 c).
\end{aligned} \tag{18}$$

Thus, the system defined by (12)-(17) is

$$\begin{bmatrix}
x_1 & -x_2 & -x_3 & 0 & 0 & 0\\
0 & x_4 & x_5 & -x_6 & -x_7 & 0\\
0 & 0 & 0 & x_8 & x_9 & -x_{10}\\
x_{11} & -x_{12} & -x_{13} & 0 & 0 & 0\\
0 & x_{14} & x_{15} & -x_{16} & -x_{17} & 0\\
0 & 0 & 0 & x_{18} & x_{19} & -x_{20}
\end{bmatrix}
\begin{bmatrix} C_1\\ C_2\\ C_3\\ C_4\\ C_5\\ C_6 \end{bmatrix} =
\begin{bmatrix} 0\\ 0\\ 0\\ 0\\ 0\\ 0 \end{bmatrix} \tag{19}$$

The constants C_2-C_6 are:

$$C_2 = C_1 \frac{(x_1 x_{13} - x_3 x_{11})}{x_2 x_{13} - x_{12} x_3}, \tag{20}$$

$$C_3 = C_1 \frac{(x_2 x_{11} - x_1 x_{12})}{x_2 x_{13} - x_{12} x_3}, \tag{21}$$

$$C_4 = \frac{d_1 x_{17} - d_2 x_{17}}{x_6 x_{17} - x_{16} x_7},$$

$$\text{where } d_1 = C_2 x_4 - C_3 x_5 \text{ e } d_2 = C_2 x_{14} - C_3 x_{15}, \tag{22}$$

$$C_5 = \frac{d_2 x_6 - d_1 x_{16}}{x_6 x_{17} - x_{16} x_7}, \tag{23}$$

$$C_6 = \frac{C_4 x_8 - C_5 x_9}{x_{10}}. \tag{24}$$

The system (19) possesses a nontrivial solution if and only if the determinant of [x] is null, i.e.

$$\det[x]=0 \tag{25}$$

This is the eigenvalue equation and its solution gives the eigenvalue γ_1. The parameters γ_2- γ_4 expressed as functions of γ_1 are:

$$\lambda_2^2 = \lambda_1^2 + \omega^2\mu_0(\varepsilon_2 - \varepsilon_1), \tag{26}$$

$$\lambda_3^2 = \lambda_1^2 + \omega^2\mu_0(\varepsilon_3 - \varepsilon_1), \tag{27}$$

$$\lambda_4^2 = \lambda_1^2 + \omega^2\mu_0(\varepsilon_4 - \varepsilon_1). \tag{28}$$

For the solution of (25), equations (26)-(28) are normalized as follows:

$$\lambda_1 a = \xi, \tag{29}$$

$$\lambda_2 a = \sqrt{\xi^2 + (k_0 a)^2(\varepsilon_{R2} - \varepsilon_{r1})}, \tag{30}$$

$$\lambda_2 b = \left(\frac{b}{a}\right)\sqrt{\xi^2 + (k_0 a)^2(\varepsilon_{R2} - \varepsilon_{r1})}, \tag{31}$$

$$\lambda_3 b = \left(\frac{b}{a}\right)\sqrt{\xi^2 + (k_0 a)^2(\varepsilon_{R3} - \varepsilon_{r1})}, \tag{32}$$

$$\lambda_3 c = \left(\frac{c}{a}\right)\sqrt{\xi^2 + (k_0 a)^2(\varepsilon_{R3} - \varepsilon_{r1})}, \tag{33}$$

$$\lambda_4 c = \left(\frac{c}{a}\right)\sqrt{\xi^2 + (k_0 a)^2(\varepsilon_{R4} - \varepsilon_{r1})}, \tag{34}$$

where $k_0 = \omega\sqrt{\mu_0\varepsilon_0}$,$\varepsilon_{R2} = \varepsilon_{r2} + \frac{\sigma_2}{j\omega\varepsilon_0}$, $\varepsilon_{R3} = \varepsilon_{r3} + \frac{\sigma_3}{j\omega\varepsilon_0}$

and ε_{R4}=1. Substituting (29)-(34) in (25), the resulting equation becomes a function of ξ. As the elements of the matrix [x] are complex, the solutions ξ are also complex numbers, with the real part ξ_r and the imaginary part ξ_i . With these notations, (25) is a system of two equations and two unknowns, ξ_r and ξ_i.

$$\begin{cases} F_1(\xi_r, \xi_i) = \mathrm{Re}(\det[x]) = 0\\ F_2(\xi_r, \xi_i) = \mathrm{Im}(\det[x]) = 0 \end{cases}. \tag{35}$$

The solutions of (35) are the points where the curves F_1 and F_2 are crossed.

III. ANALYSIS BY FEMLAB

This section presents some details of the 2D FEMLAB model. The well-known Finite Element Method (FEM) is used in this software [4].

The goal of these calculations is the current density distributions over the OPGW cross-section for different frequencies. Two geometric variants of the cable's cross-section are used in our analysis. The first variant is the geometry of Fig. 1 and the second is a modification presented in Fig. 3

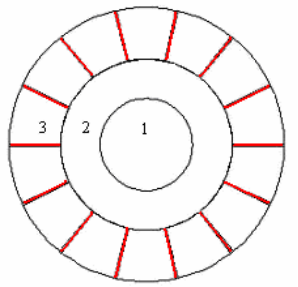

Fig. 3. A modification of the cable's cross-section.

The physical parameters used in these structures are given in Table 3.

TABLE 3
PARAMETERS USED IN STRUCTURE OF FIGURES 1 AND 3

Layer	Material	Conductivity (S/m) (σ)	Relative permittivity	Radius (mm)
1	Quartz	$1*10^{-14}$	4.2	2.35
2	Aluminum	$3.774*10^{7}$	1	4.35
3	Steel	$4.032*10^{6}$	1	7

For FEMLAB simulations, the idea of the virtual surface current density (J_V) in the outer metal layer is used.

$$J_V = -\frac{I_t}{2\pi R} \tag{36}$$

where I_t is the total real current and R the radius of the cable.

The details of the discretization for FEMLAB simulations are shown in Fig. 4.

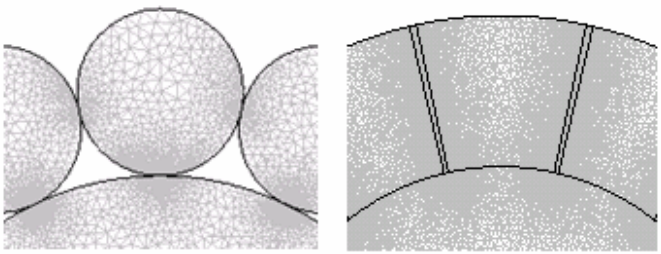

Fig. 4. Details of the discretization used in FEMLAB.

V. NUMERICAL RESULTS

The OPGW cable has a rather complex structure because it is nonhomegeneous in the radial and the azimuthal directions. Thus, the analytical model presented in Sec. 2 is a helpful tool for the investigations. The variation of the current density, J_z, as a function of the radial coordinate, ρ, of the waveguide is given in Figs. 5 and 6. These figures show the results calculated by the analytical model and by the FEMLAB software.

These results show that at the frequency of 1 kHz, and below this value, the current distribution is approximately constant with respect to ρ in the regions with the parameters shown in Tables 2 and 3. In the low frequencies (f < 1 kHz), there is no skin effect. At the frequency of 5 kHz, the skin effect appears.

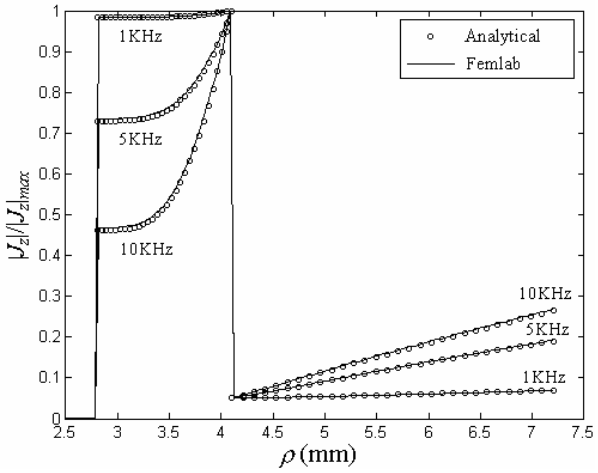

Fig. 5. Normalized magnitude of the longitudinal current J_z versus radial coordinate for different frequencies.

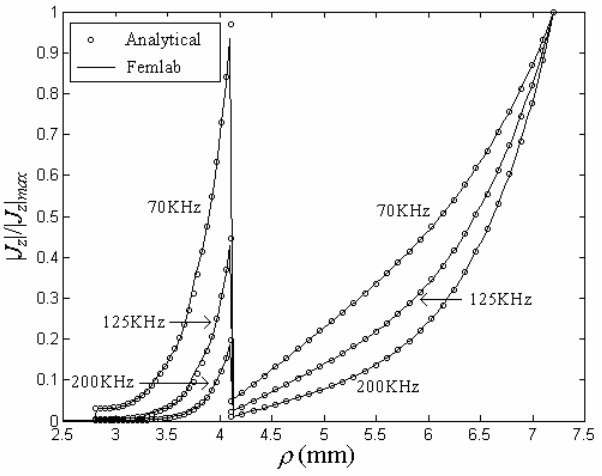

Fig. 6. Normalized magnitude of the longitudinal current J_z versus radial coordinate for different frequencies.

The distribution of current density in the cross section of the cables of Figs.1 and 3 were also calculated by FEMLAB for the frequency of 500 kHz [5]. The regions of the structure in blue color indicate the minor concentration of current density, the green color indicates the intermediate level of the current density, and the red shows the maximum current density.

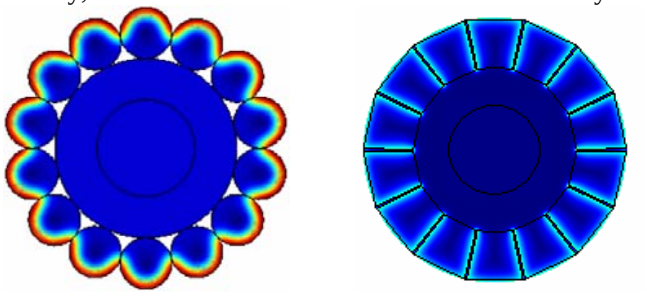

(a) (b)

Fig. 7. Current density distributions over cross-section for the basic model (a) and for the modified variant (b).

VI. CONCLUSIONS

The main results of this work are as follows: an analytical waveguide model and computational program which allow the calculation of the electromagnetic fields and current distributions in cables consisting of azimuthally uniform layers with non-ideal materials, i.e. metals with finite conductivity and dielectrics with losses, was developed. This model allows, in particular, the investigation of the skin effect and the electromagnetic fields inside and outside of the cables. The analytical results and those obtained by Finite Element Method using the commercial program FEMLAB were compared, and the results obtained are in good agreement.

Two variants of practical OPGW cables were also analyzed, using the software FEMLAB to calculate the longitudinal current density distributions over the cross-section of the cables.

REFERENCES

[1] Femlab software, website: http://www.comsol.com/.

[2] K. Q. da Costa, V. Dmitriev, J. T. Pinho, S. Colle, L. Gonzalez, M. A. Andrade, J. C. V. da Silva, and M. Bedia, "Analytical model for calculation of current density distributions over cross-section of a multi-conductor cable", *2006 IWCS/Focus Conference*, Providence, USA.

[3] J. Franc, Z. Miro, T. Igor, and U. Ivo, "Distribution of current density in layers of overhead bare conductors", *Power System and Communications Infrastructures for the Future*, 2002.

[4] John L. Volakis, Arindam Chatterjee, Leo C. Kempel, *Finite Element Method for Electromagnetics: Antennas, Microwaves Circuits, and Scattering Applications*, New York: IEEE Press, 1998.

[5] K. Q. da Costa, V. Dmitriev, J. T. Pinho, S. Colle, L. Gonzalez, M. A. Andrade, J. C. V. da Silva, and M. Bedia, "Numerical calculation of current density distributions over cross-section of OPGW cable", *Compumag 2007*, Aachen, Germany.